Biomacromolecules

pubs.acs.org/Biomac

Article

Development of Thermostable and Immunogenic Block Copolymer Nanoparticles (BNPs) for mRNA Delivery

Jian Hang Lam, Gaurav Sinsinbar, Ser Yue Loo, Teck Wan Chia, Yan Jun Lee, Jing Yi Fong, Yoong Eng Chia, Rocco Roberto Penna, Shaoqiong Liu, Steve Pascolo, Katherine Schultheis, and Madhavan Nallani*

Cite This: https://doi.org/10.1021/acs.biomac.4c01820

Read Online

ACCESS | Metrics & More | Article Recommendations | Supporting Information

ABSTRACT: Combining an amphiphilic block copolymer polybutadiene-*b*-poly(ethylene glycol) (PBD-*b*-PEO), an ionizable lipid, a helper lipid, and cholesterol produces thermostable BNPs. Luciferase mRNA-BNPs can be stored for over 1 year at 4 °C with no evidence of degradation to the mRNA or nanocarrier. In vivo, mRNA-BNPs exhibit a greater affinity for secondary lymphoid organs than mRNA-lipid nanoparticles (LNPs) and are efficiently taken up by macrophages and dendritic cells. Freshly fabricated ovalbumin (OVA) mRNA-BNPs elicit robust OVA-specific IgG and functional memory $CD8^+$ T cells that persist for at least 5 months. Immunogenicity remains intact after 24 weeks of storage at 4 °C. Anti-PEG antibodies are not boosted by the repeated administration of mRNA-BNPs, unlike mRNA-LNPs. Syrian hamsters vaccinated with SARS-CoV-2 spike mRNA-BNPs are protected against weight loss associated with infection and potently suppress pulmonary viral loads. Protective efficacy is comparable to that conferred by a Comirnaty biosimilar. Cumulatively, mRNA-BNPs are thermostable, immunogenic and possess the potential for clinical application.

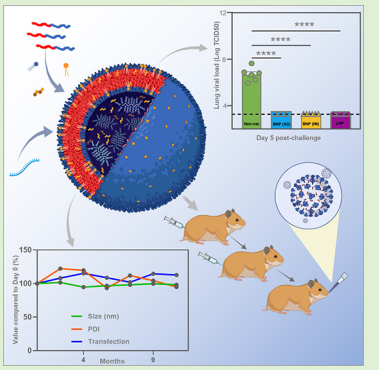

INTRODUCTION

COVID-19 vaccines of different modalities (mRNA, recombinant protein, nonreplicating viral vector and inactivated virus) are safe and effective tools for the prevention of severe disease and death caused by the etiological agent SARS-CoV-2.[1] Among them, the mRNA-LNP vaccines BNT162b2 and mRNA-1273 produced by Pfizer/BioNTech and Moderna, respectively, have distinguished themselves by efficacies of more than 90%.[2−5] LNPs are widely considered the best-in-class given their highly efficient delivery of RNA.[6,7] However, their thermal instability necessitates storage at subzero temperatures and severely restricts the duration of use at elevated temperatures. For example, unopened vials of BNT162b2 and mRNA-1273 are stable up to 6 months when frozen at −70 and −20 °C, respectively, 1 month at 2−8 °C, but only 4−24 h when kept at room temperature.[8,9] Repeated freeze−thaw cycles must be avoided to prevent potential aggregation and loss of function, though this problem may be alleviated by the addition of a cryoprotectant such as trehalose and sucrose.[10] Stringent cold-chain requirements for the storage and transport of mRNA-LNP vaccines limit their distribution to regions with well-developed infrastructure. Optimizing LNPs for long-term stability without the need for subzero storage is therefore crucial to address the distribution aspect of mRNA vaccines inequity.[11]

Lyophilization is extensively used in the pharmaceutical industry to improve stability and shelf life of many medications.[10] Other advantages include reduction in sample weight and volume for ease of shipping, and the flexibility to reconstitute at a desired concentration to facilitate dose adjustment.[9] However, it is not straightforward to apply this process to LNPs. Particles that have been lyophilized in their original formulation medium cannot be reconstituted in deionized water without a substantial loss of efficacy.[10] Instead, careful selection of lyophilization buffers, cycle process parameters and temperatures, and concentrations of cryoprotectant and LNPs is crucial for prolonged stability at 4 °C or room temperature without significant degradation of the nanocarrier, RNA payload, and functionality.[9,12,13]

Lipid membranes have conventionally been demonstrated to exhibit increased fluidity and permeability, factors that may significantly affect the stability of LNPs. The incorporation of polymers with lipids has been demonstrated to diminish both the membrane fluidity and permeability. These hybrid systems can facilitate enhanced stability, regulated and precise drug release, substantial cargo loading, targeted delivery, biocompatibility, and membrane fusion with cellular membranes, among other benefits.[14−16] We have previously utilized a polymer−lipid hybrid system for the encapsulation of SARS-CoV-2 spike

Received: December 23, 2024
Revised: March 23, 2025
Accepted: March 24, 2025

protein and CpG oligodeoxynucleotides[17,18] and the formulation was clinically evaluated in a Phase 1 trial for a COVID-19 booster vaccine (ClinicalTrials.gov identifier: NCT05385991). This polymer−lipid hybrid system exhibited thermal stability for a period of 33 months at a temperature of 4 °C (data not published). In this study, we hypothesize that combining amphiphilic block copolymer PBD-*b*-PEO with an ionizable lipid, a helper lipid, and cholesterol, as opposed to a standard LNP composition, would improve the overall mechanical stability of the nanoparticles. The resulting block copolymer nanoparticle (BNP) formulation exhibits improved thermal stability compared to LNPs and can be stored in liquid format for up to 13 months at 4 °C with no change to its morphology and in vitro transfection. Furthermore, in vivo studies show that aged OVA mRNA-BNPs remain highly immunogenic and elicit vigorous and durable OVA-specific B and T cell responses. Luciferase (Luc) mRNA-BNPs are expressed preferentially by secondary lymphoid organs after intramuscular (IM) or intravenous (IV) administration, which contrasts sharply with LNPs' potent targeting of the liver. Despite their immunogenicity, BNPs are inefficient at boosting anti-PEG antibodies and hence potentially suitable for repeated administrations. Consecutive doses of LNPs, on the other hand, significantly boost anti-PEG antibodies, which are reported to trigger accelerated drug clearance and hypersensitivity reactions.[19] Based on these encouraging results, we then proceed to test the protective efficacy of spike mRNA-BNPs in a hamster model of SARS-CoV-2 infection and show it to confer robust protection comparable to that generated by spike mRNA-LNPs. This demonstrates a potential clinical application for the BNP formulation.

MATERIALS AND METHODS

Fabrication (Materials, Processes, and Physicochemical Properties). CleanCap OVA mRNA with unmodified bases was purchased from Trilink Biotechnologies, Inc. EZ Cap Firefly Luc mRNA containing 5-methoxyuridine-5′-triphosphate was purchased from ApexBio Technology. SARS-CoV-2 N1-methylpseudouridine spike mRNA was synthesized and provided by Professor Steve Pascolo's team from University Hospital of Zurich. 4-(dimethylamino)-butanoic acid, (10Z,13Z)-1-(9Z,12Z)-9,12-octadecadien-1-yl-10,13-nonadecadien-1-yl ester (DLin-MC3-DMA) was purchased from TargetMol Chemicals Inc. 1,2-distearoyl-*sn*-glycero-3-phosphocholine (DSPC) and 1,2-dimyristoyl-rac-glycero-3-methoxypolyethylene glycol-2000 (DMG-PEG 2000) were purchased from Avanti Polar Lipids. Cholesterol was purchased from Lipoid GmbH. 1,1′-dioctadecyl-3,3,3′,3′-tetramethylindodicarbocyanine, 4-chlorobenzenesulfonate salt (DiD) and Quant-iT RiboGreen RNA Reagent and Kit were purchased from Thermo Fisher Scientific. Triton X-100 was purchased from Promega. All other chemicals were purchased from Sigma-Aldrich unless stated otherwise. LNPs (Onpattro formulation) and BNPs encapsulating Luc or OVA mRNA were prepared in-house using a microfluidic device. To fabricate LNPs (Onpattro formulation), DLin-MC3-DMA, DSPC, cholesterol, and DMG-PEG 2000 were mixed in the molar ratio of 49.3:10.1:39.0:1.6. OVA mRNA was diluted in the 20 mM sodium acetate buffer, pH 5.0. Briefly, all of the lipids were dissolved in ethanol and mixed with the mRNA solution at a flow rate ratio (FRR) of 1:3 and a total flow rate (TFR) of 12 mL/min. The sample was dialyzed against 20 mM Tris-acetate and 5% sucrose, pH 7.4, overnight, to buffer exchange and remove ethanol. The dialyzed sample was filtered through a 0.22 μm sterile syringe filter. BNPs were prepared by mixing Dlin-MC3-DMA, DSPC, cholesterol, and our proprietary block copolymer PBD-*b*-PEO in the molar ratio of 49.3:10.1:39.0:1.6. The block copolymer has the molecular formula PBD_{22}-*b*-PEO_{13}, molecular weight of 1800 Da, PEG length of 600 Da and polydispersity index (PDI) of 1.04. It was previously described for the fabrication of polymersomes to deliver SARS-CoV-2 spike protein and CpG oligodeoxynucleotides.[17,18] All four lipid components were prepared in ethanol and mixed with an mRNA solution (in 20 mM sodium acetate buffer, pH 5.0) using a NanoAssemblr Ignite system (Precision NanoSystems) at a FRR of 1:3 and TFR of 12 mL/min. The sample was buffer exchanged into 20 mM Tris-acetate buffer, and ethanol was removed using a centrifugal concentrator. This facilitated the quick switch of pH from acidic to neutral needed for BNP manufacture, which could not be achieved by using simple dialysis. LNPs, on the other hand, were dialyzed to avoid shear stress caused by centrifugal filtration. LNPs were fabricated with an N/P ratio of 4 while BNPs were fabricated with an N/P ratio of 10. BNPs were eventually filtered through a 0.22 μm sterile syringe filter. Particle sizes were characterized by dynamic light scattering (DLS) using a Zetasizer ZSP Nano instrument from Malvern Panalytical Ltd. Intensity-based size distribution measurements were performed for one LNP and one BNP sample at each time point for up to 13 months. Triplicate measurements with 10 runs each were conducted at a 173° backscattering detection angle. The sample was diluted 50-fold using 20 mM Tris-acetate, 5% sucrose, pH 7.4 buffer and vortexed for 3 s before transferring into the cuvette. Concentrations of mRNA for one LNP and one BNP sample were determined in triplicate using the RiboGreen kit at each time point for up to 13 months. Nanoparticles were lysed with 3.3% v/v Triton X-100 for 15 min at 37 °C for the determination of total mRNA. This protocol was derived from an optimization study to identify detergent concentration and reaction condition that resulted in complete lysis of PBD-*b*-PEO nanoparticles. Complete lysis was confirmed by DLS which showed the loss of peak corresponding to intact LNPs or BNPs (Figure S1). A standard curve was prepared using purified Luc or OVA mRNA treated with Triton X-100 in the manner above to account for interference by the detergent in the RiboGreen assay. Nonencapsulated mRNA was determined from intact nanoparticles against mRNA standards that were not treated with Triton X-100. The encapsulated mRNA concentration was calculated by the following formula: (total mRNA) - (nonencapsulated mRNA). Encapsulation efficiency (EE) was calculated by the following formula: (encapsulated mRNA)/(total mRNA) × 100%. DiD-labeled OVA mRNA-LNPs and BNPs were prepared by doping 1% DiD dye in the lipid-ethanol stock solution and following the respective methods described above. The endotoxin amount in the samples was measured by the Kinetic-QCL Kinetic Chromogenic LAL Assay (Lonza). Fabrication of the Comirnaty biosimilar used in the hamster experiment was performed by a third-party service provider (Helix Biotech, Inc., USA) using lipids and reagents supplied by said facility. ALC-0315, DSPC, cholesterol, and ALC-0159 were added in the molar ratio of 46.3:9.4:42.7:1.6. mRNA (in 100 mM NaOAc buffer, pH 5.0) and lipids (in ethanol) were mixed using a turbulent impinged jet mixer system (IJM; Nova BT, Helix Biotech) to induce flash nanoprecipitation (FNP) of LNPs at the FRR of 5:1, TFR of 18 mL/min and N/P ratio of 6. LNPs were dialyzed against PBS, pH 7.4 at 4 °C. Physicochemical evaluation revealed a particle size of 58.4 nm, PDI of 0.17, mRNA loading of 100 μg/mL and EE of >90% after sterile filtration. Unless stated otherwise, formulations were characterized and used within 2 weeks of fabrication.

In Vitro Transfection. Cell culture reagents were purchased from Thermo Fisher Scientific, unless stated otherwise. HEK293T cells (CRL-3216, ATCC) were cultured in RPMI 1640 supplemented with 10% v/v heat-inactivated fetal bovine serum, 2 mM L-glutaMAX and 1× Pen/Strep. The cell line was kept within 30 passages. The transfection efficiency of one Luc mRNA-LNP sample and one Luc mRNA-BNP sample was evaluated at each time point for up to 13 months using HEK293T seeded in triplicate at 25,000 cells per well in a 96-well plate. Cells were incubated for 18−24 h at 37 °C, 5% CO_2, prior to transfection. Luc mRNA complexed with Lipofectamine MessengerMAX (Thermo Fisher Scientific) served as standards for the transfection assay. Briefly, mRNA and MessengerMAX were individually diluted in OPTI-MEM (Thermo Fisher Scientific) and left to stand for 5 min. They were then mixed and further incubated for another 5 min before applying to cells. 100 ng of Luc mRNA-

https://doi.org/10.1021/acs.biomac.4c01820
Biomacromolecules XXXX, XXX, XXX−XXX

LNPs or Luc mRNA-BNPs were diluted in OPTI-MEM before adding to the cell culture. 18−24 h post-transfection, the ONE-Glo + Tox luciferase reporter and cell viability assay kit (Promega) was used according to manufacturer's instructions. Briefly, 20 μL of 5× cell titer-fluor reagent were added to cells and incubated for 30 min at 37 °C in a humidified CO_2 incubator. Fluorescence representing cell viability was measured on Biotek Plate reader at 400 nm Ex/525 nm Em; 100 μL of ONE-Glo Reagent were then added to cells and incubated for 1 min at room temperature. Luc expression was calculated in terms of relative luminescence units normalized to cell viability in relative fluorescence units (i.e., RLU/RFU). For long-term monitoring of Luc expression by mRNA-LNPs and mRNA-BNPs, normalization to 25 ng of Luc mRNA transfected using the MessengerMAX reagent was performed at each time point.

Animals and Ethics Statements. All animal studies were performed in accordance with protocols approved by the Institutional Animal Care and Use Committee (IACUC) of the Agency for Science, Technology and Research (A*STAR), Singapore, the Wenzhou Institute, University of Chinese Academy of Sciences, China, or Bioqual, Inc., USA. For cellular uptake and immunogenicity studies, female C57BL/6 mice were purchased from InVivos Pte Ltd. (Singapore), housed at the AAALAC-accredited Biological Resource Center (BRC), A*STAR, Singapore, and used at 9−10 weeks of age. For bioluminescence imaging studies, female C56BL/6 mice were provided by the Zhejiang Experimental Animal Center, China, housed at the Wenzhou Institute, University of Chinese Academy of Sciences, China, and used at 6−8 weeks of age. For SARS-CoV-2 studies, Golden Syrian hamsters of both genders were housed at the Bioqual vivarium facility and used at 6−8 weeks of age. Upon receipt, all animals were acclimated at least 3 days before the start of any study.

Injections. Mice were anesthetized with 3% isoflurane prior to injection. Formulations were administered using 1 mL Tuberculin syringes affixed with 30 G needles (BD). IM administration was performed at the rear thigh muscle with a 50 μL injection volume. IV administration was performed at the retro-orbital sinus by the method of Yardeni et al.[20] or at the tail vein with a 100 μL injection volume. Hamsters were shaved at the injection site 1 day prior to subcutaneous (SC; scruff of the neck) or IM (hind leg) administration. LNP and BNP formulations were injected in a volume of 100 μL. OVA mRNA and SARS-CoV-2 spike mRNA were administered at a dose of 5 μg (i.e., 50 μg/mL in 100 μL injection volume). Luc mRNA was administered at a dose of 7 μg (i.e., 70 μg/mL in 100 μL injection volume).

SARS-CoV-2 Challenge (Hamsters Only). Animals were anesthetized with a ketamine (80 mg/kg)/xylazine (5 mg/kg) mixture prior to intranasal (IN) administration of the SARS-CoV-2 USA/NY-PV08449/2020 (D614G) strain at a dose of 5×10^7 $TCID_{50}$ in 100 μL, distributed equally between both nares. Animals were positioned upright with snouts facing upward and the viral inoculum was administered dropwise using a P200 pipettor. Animals were monitored 20 min before antisedan (1 mg/kg) was administered to reverse the anesthesia. Body weight measurements and clinical observations were performed once and twice, respectively, each day during the challenge period. Weight loss of ≥20% baseline body weight constituted a humane end point. On Day 5 post challenge, 60% of hamsters per group were sacrificed after weight measurement for the determination of viral loads in their lungs.

Determination of Infectious Viral Load in the Lungs. Vero E6 cells were plated at 20,000 cells per well in DMEM + 10% FBS + gentamicin and incubated at 37 °C, 5% CO_2 to achieve 80−100% confluency. The spent culture medium was removed, and cells were overlaid with lung homogenate serially diluted 10-fold with DMEM + 2% FBS + gentamicin. Cells were further incubated for 4 days and then visually inspected for cytopathic effect (CPE). The presence and absence of CPE were recorded as (+) and (−), respectively, and the $TCID_{50}$ was calculated using the Reed−Muench formula.

In Vivo Expression of Luc mRNA. LNPs and BNPs encapsulating Luc mRNA were administered IV or IM to mice at 7 μg of mRNA per animal, and their organ expression was monitored using bioluminescence imaging. Negative control mice were administered PBS. At 6 h post administration, mice were administered D-luciferin (Glpbio) at a dose of 150 mg/kg intraperitoneally. Mice were anesthetized in a chamber with 3% isoflurane and placed on the imaging platform while being maintained on 2% isoflurane via a nose cone. Mice were imaged at 5 min post administration of D-luciferin with the IVIS Spectrum imaging system (IVIS Lumina XRMS Series III, PerkinElmer) using an exposure time of 30 s or longer to ensure that the signal acquired was within the effective detection range (above noise levels and below CCD saturation limit). Animals were eventually sacrificed and their organs/tissues (i.e., heart, liver, spleen, lung, kidney, pancreas, inguinal lymph node, and thigh muscle) were harvested for ex vivo imaging. Bioluminescence values were quantified by measuring photon flux (photons/second) in the region of interest where the bioluminescence signal emanated using the Living IMAGE Software (Living Image Version 4.5) provided by PerkinElmer.

Evaluating the Immunogenicity of mRNA Vaccines in Hamsters. Five male and five female hamsters were randomized into each vaccination group. Five μg of mRNA encoding ancestral SARS-CoV-2 spike was formulated in BNPs or LNPs (Comirnaty biosimilar) and injected SC or IM on Days 0 and 21. Blood was obtained on Days 14 and 34 to determine antispike IgG titers after one and two doses, respectively. Animals were anesthetized by inhalation of 2−5% isoflurane and blood was collected via the retro-orbital route.

Anti-OVA IgG ELISA. Purified OVA protein (Worthington Biochemical Corporation) was solubilized in 1X PBS (1st BASE) to a working concentration of 10 μg/mL and applied to a 96-well flat bottom EIA/RIA high binding plate (Corning) at 100 μL per well. Coating was done at 4 °C, overnight. The plate was then washed three times with 0.1% v/v Tween-20 in 1× PBS and blocked with 2% w/v BSA (Sigma-Aldrich) in wash buffer for 2 h at room temperature. Sera were diluted 1:100 with blocking buffer followed by 4-fold serial dilutions to a final of 1:1,638,400 and applied at 100 μL per well for 2 h at room temperature. HRP-conjugated goat antimouse IgG (H/L) (Bio-Rad) was diluted 1:10,000 with blocking buffer and applied at 100 μL per well for 1 h at room temperature. Antibody binding was visualized by the addition of a supersensitive TMB substrate (Sigma-Aldrich) for 10 min at room temperature in the dark. The reaction was stopped by an equal volume of ELISA Stop Solution (Thermo Fisher Scientific) and the optical density of the yellow product was measured at 450 nm using the BioTek Synergy H1 Reader (Agilent). A titration curve was generated using 5-parameter nonlinear regression using GraphPad Prism version 10.2.2 and antibody titer, defined as the highest dilution factor that generated an absorbance 3× of background, was interpolated.

Anti-PEG IgG and IgM ELISA. The protocol was adapted from Yang et al.[21] with modifications. Sera were diluted 1:10 with blocking buffer (1% w/v skim milk in 1× PBS) followed by 3-fold serial dilutions to a final of 1:43,740 and applied at 100 μL per well of a mono-PEGylated (20 kDa mPEG) BSA-precoated plate (Life Diagnostics Inc.) for 2 h at room temperature. The plate was washed thrice with PBS before HRP-conjugated goat antimouse IgG (H/L) or HRP-conjugated goat antimouse IgM heavy chain (Thermo Fisher Scientific) were diluted 1:10,000 and 1:4000, respectively, and applied at 100 μL per well for 1 h at room temperature. The antibody titer was determined as described above.

Preparation of Peripheral Blood Leukocytes (PBLs), Spleen, and Liver for Flow Cytometry. Approximately 100 μL of whole blood was collected in 30 mM EDTA (1st BASE) to prevent coagulation. Cells were resuspended in 1 mL of 1× RBC Lysis Buffer (Thermo Fisher Scientific) and incubated for 10 min at room temperature. Intact cells were pelleted at 400 g at 4 °C for 4 min and washed once with FACS buffer (1× PBS + 2% v/v heat inactivated FBS + 1 mM EDTA). For the monitoring of DiD-labeled particle uptake by the spleen and liver, mice were freshly sacrificed by CO_2 asphyxiation and perfused at the left ventricle of the heart with 3 mL of digestion buffer [RPMI 1640 + 0.2 mg/mL Type IV collagenase (Thermo Fisher Scientific) + 10% v/v heat inactivated FBS] prior to organ harvest. The spleen was mechanically ground through a 70 μm cell strainer (SPL Life Sciences) using the plunger of a 3 mL syringe

https://doi.org/10.1021/acs.biomac.4c01820
Biomacromolecules XXXX, XXX, XXX−XXX

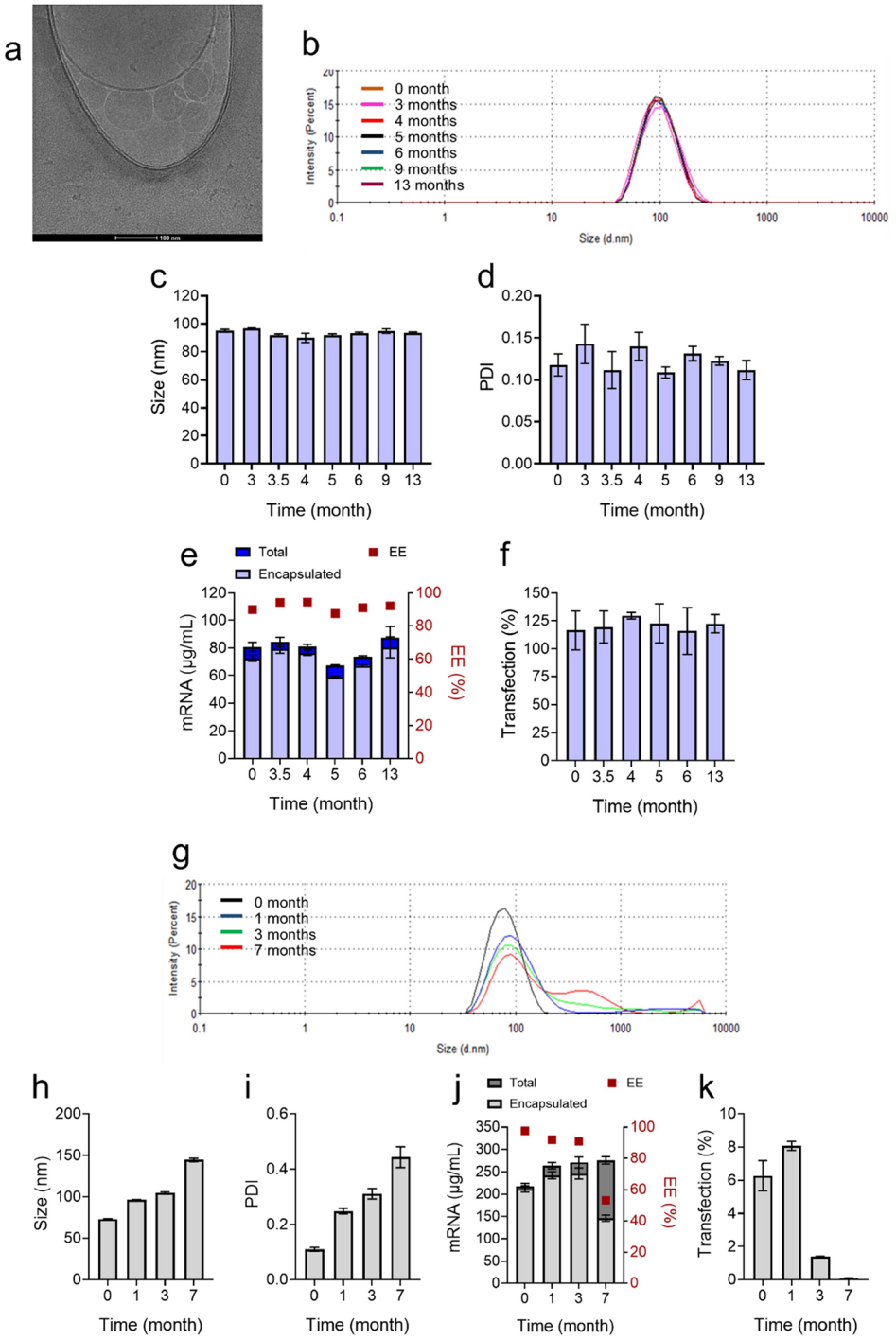

Figure 1. Physicochemical characteristics and transfection efficiencies of Luc mRNA-BNPs and Luc mRNA-LNPs after prolonged storage at 4 °C. (a) Representative cryo-TEM image of Luc mRNA-BNPs after removal of ethanol and buffer exchange. Scale bar corresponds to 100 nm. (b) Intensity-weighted size distribution of BNPs measured by the DLS particle analyzer for up to 13 months. (c–f) Particle size, PDI, total mRNA, encapsulated mRNA, EE and transfection efficiency of BNPs across 13 months. (g) Intensity-weighted size distribution of LNPs for up to 7 months. (h–k) Particle size, PDI, total mRNA, encapsulated mRNA, EE and transfection efficiency of LNPs across 7 months. One BNP and an LNP sample were monitored. Mean ± SD from three technical replicates at each time point is presented. Luc expression by BNPs and LNPs was normalized to 25 ng of Luc mRNA transfected using the MessengerMAX reagent at each time point.

to obtain a single cell suspension in FACS buffer. The liver was finely minced with a pair of scissors, incubated in 2 mL of digestion buffer for 1 h at 37 °C and ground through a 70 μm cell strainer to obtain a single cell suspension in FACS buffer. Erythrocytes were lysed using the method above. Samples were stained with Trypan Blue to exclude dead cells, and viable counts were manually determined using a hemocytometer.

Peptide Restimulation. Cell culture reagents were purchased from Thermo Fisher Scientific unless stated otherwise. Splenocytes were seeded in a 96-well U bottom plate at 2 million per well in 200 μL of complete culture medium (RPMI 1640 + 10% v/v heat-inactivated FBS + 50 μM 2-mercaptoethanol + 2 mM L-glutamax + 10 mM HEPES + 1× Pen/Strep). Cells were stimulated with 1 μg/mL SIINFEKL peptide (Sigma-Aldrich) + 1 μg/mL anti-CD28

https://doi.org/10.1021/acs.biomac.4c01820
Biomacromolecules XXXX, XXX, XXX−XXX

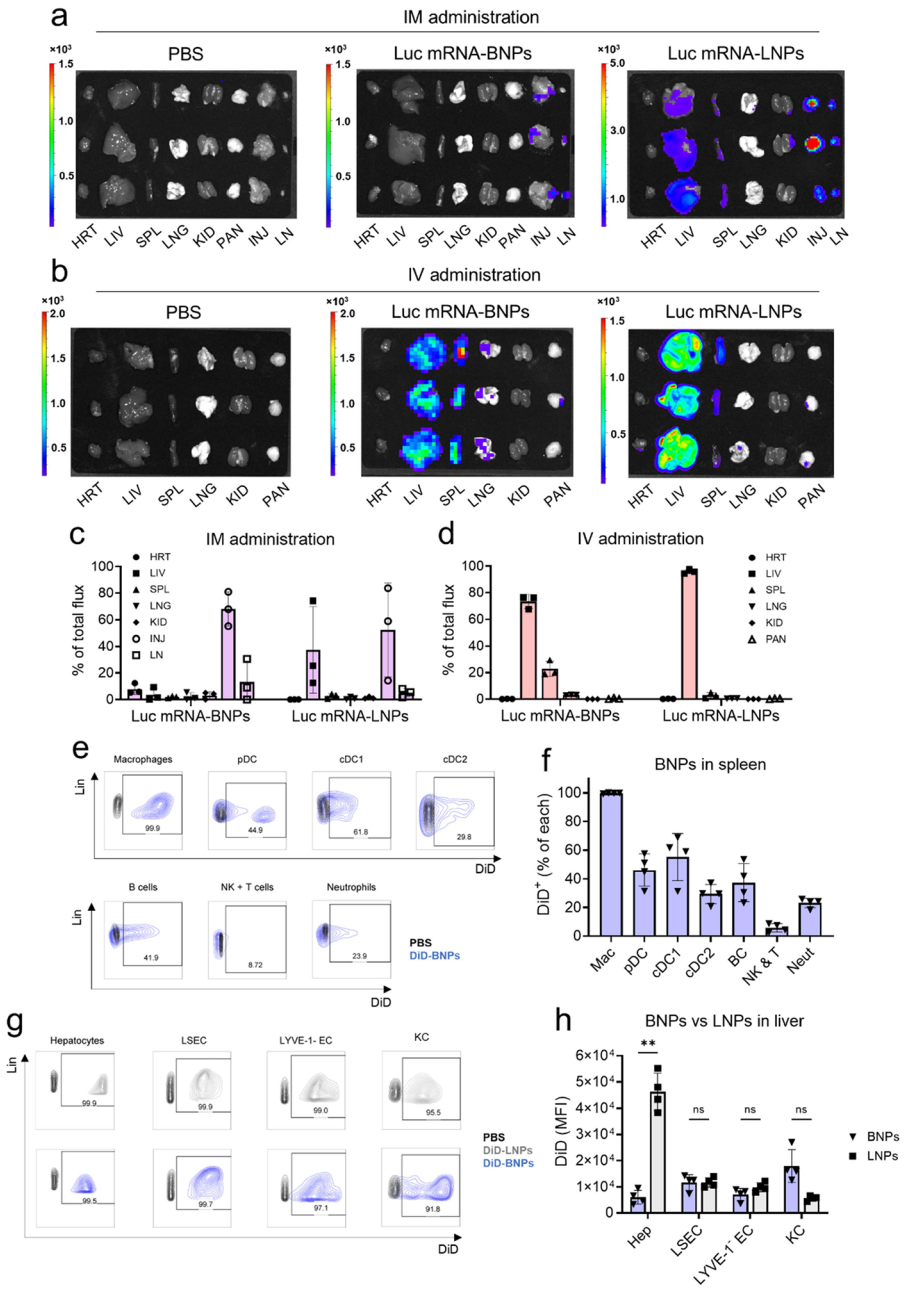

Figure 2. Organ expression and cell distribution of mRNA-BNPs. Mice were IM or IV administered freshly fabricated BNPs or LNPs encapsulating Luc mRNA. Organs were harvested 6 h later for ex vivo bioluminescent imaging. (a, b) Representative images of Luc-expressing organs. HRT, heart; LIV, liver; SPL, spleen; LNG, lungs; KID, kidneys; PAN, pancreas; INJ, injection site (thigh muscle); and LN, inguinal lymph nodes. The pancreas was not harvested during the analysis of IM administered LNPs. (c, d) Graphical summary of the proportion of Luc expression among organs. Flux of each organ was subtracted for background derived from PBS controls and expressed as a percentage of the total. Bar graphs and whiskers represent the mean ± SD (e, f) Proportions of different splenic immune cell types showing uptake of DiD-labeled BNPs and representative FACS plots. Particles were IV administered to mice (n = 4) and organs were harvested 2 h later for FACS analysis. (g, h) Mean fluorescence intensities (MFIs) of different cell types of the liver after mice were IV treated with DiD-labeled BNPs or LNPs and their representative FACS plots. Hep, hepatocytes; EC, endothelial cells; LSEC, liver sinusoidal endothelial cells; KC, Kupffer cells. Where appropriate, two-way ANOVA with Šídák's multiple comparisons test was performed. **: $P \leq 0.01$; ns, not significant.

costimulatory mAb + 1 μg/mL anti-CD49d costimulatory mAb + 1× brefeldin A (BioLegend) + 1× monensin (BioLegend), for 5.5 h at 37 °C, 5% CO_2. Unstimulated wells were incubated with the above mix sans peptide. Positive control wells were stimulated with 1× Cell Activation Cocktail (containing phorbol 12-myristate-13-acetate and ionomycin; BioLegend) + 1× brefeldin A + 1× monensin. Peptide-induced cytokine production was subtracted for the background generated by unstimulated cells.

FACS Staining and Analysis. Splenocytes and PBLs were incubated with Fixable Viability Dye eFluor 455UV (Thermo Fisher Scientific) at 1:400 in PBS for 30 min at 4 °C for live/dead discrimination. OVA-specific $CD8^+$ T cells were identified by staining with PE conjugated-H-2Kb/SIINFEKL pentamer (Proimmune) at 1:10 in FACS buffer for 15 min at room temperature. FACS antibodies were used at 1:200 in a FACS buffer. T cell surface markers were stained with the following antibody panel in FACS buffer for 30 min at 4 °C: FITC-αCD45 (30-F11; BD Biosciences), BV785-αCD3

https://doi.org/10.1021/acs.biomac.4c01820
Biomacromolecules XXXX, XXX, XXX−XXX

(17A2; BioLegend), AF700-αCD4 (GK1.5; BioLegend), APC-eFluor 780-CD8 (53−6.7; eBioscience), and PE-Dazzle 594-αCD44 (IM7; BioLegend). Splenic immune subsets were analyzed using the following panel: BUV395-αCD45 (30F11; BD Biosciences), PE-αCD3 (17A2; BioLegend), PE-αCD49b (DX5; BioLegend), BUV737-αCD19 (1D3; BD Biosciences), PE-Cy7-αLy-6G (1A8; BioLegend), BV510-αMHC-II (M5/114.15.2; BioLegend), BV785-αF4/80 (BM8; BioLegend), PE-CF594-αCD11c (HL3; BD Biosciences), PerCP-Cy5.5-αXCR1 (ZET; BioLegend), APC-Fire 750-αCD11b (M1/70; BioLegend), BV650-αB220 (RA3−6B2; BioLegend), and AF700-αCD172a (P84; BioLegend). Liver cell types were analyzed using the following panel: BUV395-αCD45 (30F11; BD Biosciences), BV785-αF4/80 (BM8; BioLegend), APC-Fire 750-αCD11b (M1/70; BioLegend), AF594-αASGPR1 (8D7; Santa Cruz Biotechnology), PE-Cy7-αCD31 (390; eBioscience), and PE-αLYVE-1 (ALY7; eBioscience). Uptake of DiD-labeled particles was detected in the APC channel. To access intracellular cytokines, cells were treated with the cytofix/cytoperm fixation/permeabilization kit (BD Biosciences), according to the manufacturer's instructions. Cells were stained with AF488-αIFNγ (XMG1.2; BioLegend) in 1× Perm/Wash buffer for 30 min at 4 °C. Cells were resuspended in FACS buffer for data acquisition with the FACSymphony A3 flow cytometer (BD Biosciences). Data analysis was done using FlowJo v10.8.1.

RESULTS

BNP is a Thermostable mRNA Delivery Platform That Can be Stored Nonfrozen without Loss of Function. Our earlier work with the PBD-*b*-PEO demonstrated its ability to confer exceptional stability to polymersomes[22] and, furthermore, mixing amphiphilic block copolymers with lipids enhanced steric stability of the monolayer or bilayer architecture of a lipid based self-assembly.[23,24] We hypothesized that incorporation of block copolymers into a predominantly lipid driven self-assembly, such as the LNP Onpattro formulation,[25] may enhance its morphological stability and thus make it less susceptible to aggregation at 4 °C in liquid format.[22] Here, we considered a low molecular weight amphiphilic block copolymer with a short PEG length of 600 Da to evaluate said effect. Accordingly, DMG-PEG 2000 was substituted by PBD-*b*-PEO while preserving the molar ratio of DLin-MC3-DMA to DSPC to cholesterol to PBD-*b*-PEO at 49.3:10.1:39.0:1.6. Intensity-weighted DLS size measurements of three independent fabrications showed an average BNP size of 95.3 ± 4.2 nm and a polydispersity index (PDI) of <0.2. Preparations were homogeneous with no evidence of phase separation. Cryogenic transmission electron microscopy (cryo-TEM) revealed largely uniform vesicles of sizes slightly lower than 100 nm, with no bleb structures seen (Figure 1a). To evaluate thermal stability, BNPs encapsulating Luc mRNA were stored in liquid format at 4 °C for up to 13 months, and physicochemical properties were monitored. DLS revealed an intensity-weighted unimodal size distribution that remained stable for up to 13 months (Figure 1b). Particle size and PDI showed minor fluctuations around the averages of 93.3 and 0.123 nm, respectively, across time points (Figure 1c,d). Total mRNA and encapsulated mRNA fluctuated slightly around the average of 79.0 and 72.4 μg/mL, respectively, across time points (Figure 1e), yielding an EE of 90%. Lower loading of BNPs (~70 μg/mL mRNA) compared to LNPs (~200 μg/mL mRNA) was due to a higher N/P ratio of 10 for BNPs versus 4 for LNPs. The maintenance of BNPs' physicochemical properties was accompanied by stable transfection of HEK293T cells (Figure 1f). When normalized against a fixed dose of 25 ng of Luc mRNA transfected using MessengerMAX reagent, 100 ng of Luc mRNA-BNPs exhibited an average transfection efficiency of 120.9% across time points. In contrast, the size distribution of mRNA-LNPs was seen to widen progressively from 0 to 3 months, specifically in the size range of 200 to 1000 nm, before the emergence of two pronounced peaks in the size range of 200−1000 nm and 4000−6000 nm at the 7th month (Figure 1g), suggesting major aggregation and structural instability. Particle size increased by 2-fold (73.1−144.3 nm) and PDI by 4-fold (0.11 to 0.44) after 7 months at 4 °C (Figure 1h,i). From 0 to 3 months, there was no evidence of a decline in total or encapsulated mRNA, though minor variations were seen across time points (217.0−270.7 and 211.6−246.0 μg/mL, respectively; Figure 1j). EE remained above 90% for up to 3 months before dropping to 53.1% at the 7th month as the encapsulated mRNA declined to 146.3 μg/mL while total mRNA remained unchanged. This suggested leakage of encapsulated mRNA that coincided with pronounced aggregation of LNPs as seen in DLS (Figure 1g). The transfection efficiency of 100 ng of Luc mRNA-LNPs was similar between 0 and 1 month (6.3 and 8.1% normalized to 25 ng of Luc mRNA transfected with MessengerMAX, respectively; Figure 1k), indicating that the mild increase in size distribution at 1 month (Figure 1g) did not impair transfection. At 3 and 7 months, transfection decreased sharply to 1.4 and 0.07%, respectively (Figure 1k). This was likely driven by marked aggregation of LNPs at the 3rd month that worsened at the 7th month and was further exacerbated by the leakage of mRNA. Overall, we demonstrated the ability of PBD-*b*-PEO to stabilize an LNP formulation at 4 °C, based on stable physicochemical properties and transfection efficiency for 13 months.

Preferential Expression of mRNA-BNPs by the Secondary Lymphoid Organs. Luc mRNA formulations were IM or IV administered to C57BL/6 mice, and organs were harvested 6 h later for ex vivo bioluminescence imaging (see Figure 2a,b, respectively, for representative images). Expression of LNPs occurred largely at the injection site (thigh muscle; 52% of total flux) but was also detected in the liver (37%) after IM administration (Figure 2c). Liver expression increased to >95% following IV injection (Figure 2d). Strong liver expression was consistent with the known biodistribution pattern of the Onpattro formulation as well as LNPs corresponding to Pfizer/BioNTech and Moderna formulations.[25−27] BNPs displayed reduced expression in the liver (3.6% after IM; 73% after IV) but increased expression in the lymph nodes (13%; Figure 2c) and the spleen (20%; Figure 2d) after IM and IV administration, respectively. These results indicated an increased affinity of BNPs for secondary lymphoid organs. To investigate the cellular distribution of BNPs within the spleen, mice were IV injected with particles labeled with the fluorescent DiD dye, thus enabling cellular uptake to be monitored by flow cytometry. The FACS antibody panel was based on the work of Liu et al.[28] and allowed for the identification of neutrophils (Ly-6G$^+$), B cells (Lin$^+$MHC-II$^+$), NK and T cells (Lin$^+$MHC-II$^-$), macrophages (Lin$^-$F4/80$^+$CD11b^{lo}), plasmacytoid dendritic cells (pDCs; Lin$^-$B220$^+$CD172a^{lo}), type 1 classical dendritic cells (cDC1; Lin$^-$F4/80$^-$CD11c$^+$MHC-II$^+$XCR1$^+$) and type 2 classical dendritic cells (cDC2; Lin$^-$F4/80$^-$CD11c$^+$MHC-II$^+$CD11b$^+$). DiD signal was detected at moderate to high levels in multiple immune subsets except NK and T cells (see Figure 2e for representative FACS plots and Figure 2f for a graphical summary). Uptake was the highest in macrophages

https://doi.org/10.1021/acs.biomac.4c01820
Biomacromolecules XXXX, XXX, XXX−XXX

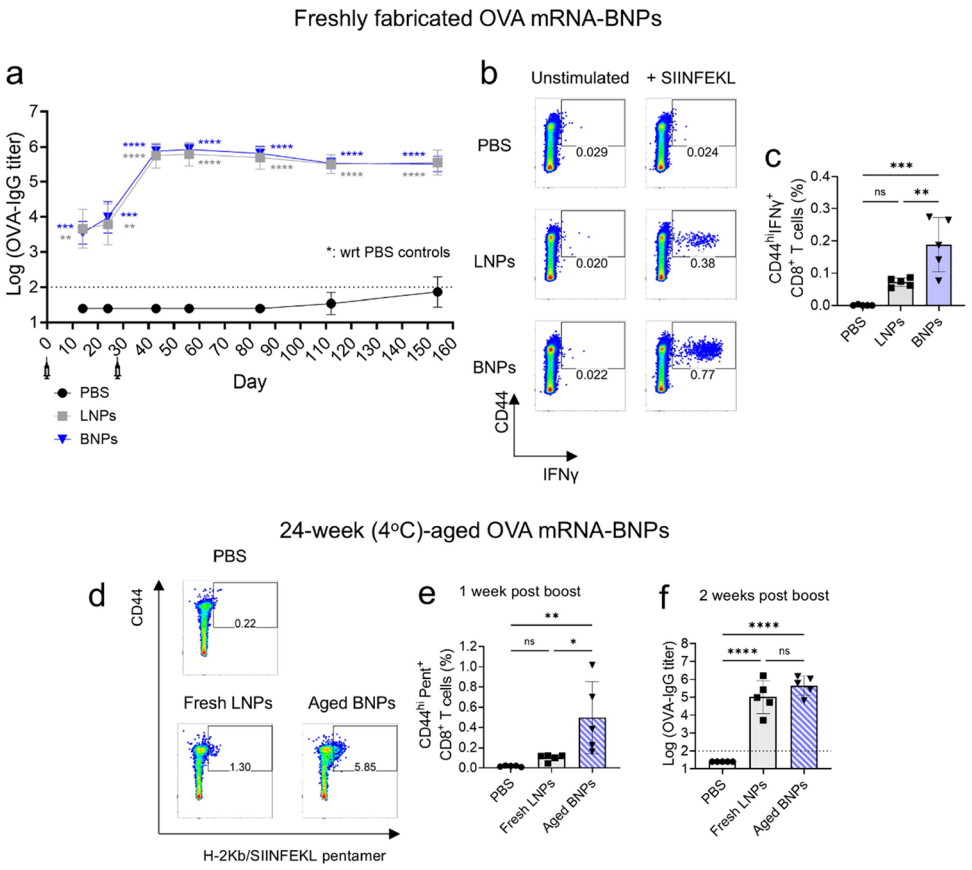

Figure 3. mRNA-BNPs were immunogenic and induced durable antigen-specific IgG and memory CD8$^+$ T cells. C57BL/6 mice (n = 5) were IM immunized two doses of freshly fabricated LNPs or BNPs encapsulating OVA mRNA (5 μg per dose), 1 month apart. (a) Anti-OVA IgG titers measured at specified time points up to Day 154. Mean ± SD is shown. Horizontal dotted line represents lower limit of detection (1:100 serum dilution). Samples below limit of detection are assigned a nominal value. Syringes below the X-axis represent immunization time points. (b) Representative FACS plots of OVA-specific, IFNγ-producing CD8$^+$ T cells on Day 154. Splenocytes were restimulated with SIINFEKL peptide and stained for intracellular cytokines. Responding cells were entirely of the CD44^{hi} memory phenotype. (c) Comparison of CD44^{hi}IFNγ^+CD8$^+$ T cells among treatment groups. Frequencies of responding T cells are expressed as percentages of viable CD45$^+$ events. Bar graphs and whiskers represent mean ± SD. (d–f) OVA mRNA-BNPs were re-evaluated after 24 weeks of storage at 4 °C. Mice were administered two doses of aged BNPs or freshly fabricated LNPs. (d) Representative FACS plots of circulating CD8$^+$ T cells 1 week post boost. Pent$^+$CD8$^+$ T cells were entirely of the CD44^{hi} memory phenotype. (e) Comparison of OVA-specific CD8$^+$ T cells generated by fresh LNPs or aged BNPs. (f) Comparison of anti-OVA IgG titers 2 weeks post boost. Where appropriate, ordinary or repeated measures one-way or two-way ANOVA with Tukey's multiple comparisons is performed. For subfigure (a), differences exist only with respect to PBS controls. *: $P \leq 0.05$; **: $P \leq 0.01$; ***: $P \leq 0.001$; ****: $P \leq 0.0001$; ns, not significant.

with >95% of the population exhibiting DiD uptake, followed by the different subsets of dendritic cells (i.e., pDCs, cDC1 and cDC2) at an average of 29–55%. Despite strong liver uptake of LNPs and BNPs in vivo, we hypothesized that their respective cellular distributions may differ in view of BNPs' higher affinity for the immune compartment. BNPs and LNPs were efficiently internalized by various cell types of the liver, with >90% of each exhibiting some degree of DiD fluorescence [see Figure 2g for representative plots of hepatocytes, endothelial cells and Kupffer cells (KCs)]. Nevertheless, marked differences in the mean fluorescence intensities (MFIs) of LNP- or BNP-treated hepatocytes (CD45$^-$ASGPR1$^+$) and KCs (CD45$^+$F4/80$^+$CD11b^{lo}) were observed. Specifically, the magnitude of LNP uptake by hepatocytes was ∼7-fold higher than that of BNP whereas the opposite trend was observed for KCs, which internalized BNPs at ∼3-fold higher efficiency than LNPs (Figure 2h). KCs exposed to DiD-labeled LNPs exhibited an MFI that ranged from 4.4×10^3 to 6.6×10^3, with an average of 5.6×10^3. In contrast, KCs exposed to DiD-labeled BNPs presented with a range of MFI (1.3×10^4 to 2.7×10^4) and an average MFI (1.8×10^4) that were substantially greater. The difference in average MFI between the two groups did not reach statistical significance, likely because of the variable uptake of BNPs compared with the uniform uptake of LNPs. Specifically, FACS plots of KCs exposed to DiD-BNPs revealed a divided uptake profile that was separated into DiD^{lo} and DiD^{hi} subsets, which contrasted with the uniform, intermediate rate by which DiD-LNPs were taken up (Figures 2g and S2a). Most of the BNP uptake (66.2%) occurred at the high level (Figure S2b), which raised the possibility of a distinct KC subset with increased affinity for BNPs. Accordingly, the phenotypic and functional heterogeneity of resident liver macrophages was only recently understood[29] and KCs were shown to exist as two subpopulations with distinct gene and protein expression patterns.[30] One marker that distinguished these two subsets was the hyaluronan receptor LYVE-1 and here we saw the DiD^{hi} subset to express LYVE-1 at a significantly greater level compared to the DiD^{lo} subset (25.1 and 2.9%, respectively; Figure S2c,d). While the experimental setup was inadequate to establish a role for LYVE-1 in the

https://doi.org/10.1021/acs.biomac.4c01820
Biomacromolecules XXXX, XXX, XXX−XXX

uptake of BNPs, these findings tentatively suggest the existence of key surface receptors that mediate BNP uptake. Given the increased expression of mRNA-BNPs by the secondary lymphoid organs, their efficient uptake by professional antigen presenting cells (APCs), and the central role of such cells in the initiation of an adaptive immune response, we next explored the use of BNPs as carriers for mRNA vaccines.

mRNA-BNPs Are Immunogenic but Do Not Boost Anti-PEG Antibodies. The immunogenicity of mRNA-BNPs was first evaluated by using a model antigen. C57BL/6 mice were IM administered two doses of freshly fabricated OVA mRNA-BNPs or LNPs, 1 month apart. The mRNA doses featured in this work fell within the range (0.1−10 μg) reported for mouse and hamster studies involving BNT162b2, mRNA-1273 and Luc mRNA-LNPs.[31−35] Notably, a dose of 1 μg mRNA-1273 was highly immunogenic in mice and hamsters and robustly protected against weight loss and viral replication after SARS-CoV-2 challenge.[34,35] Moreover, immunogenicity did not increase with an increase to 25 μg mRNA-1273 in hamsters.[35] A dose of 30−100 μg, although approved for use in humans in the context of BNT162b2 and mRNA-1273,[36] is not typically administered nor is it necessary to demonstrate immunogenicity in rodents. A single dose of LNPs or BNPs containing 5 μg of OVA mRNA generated comparable levels of anti-OVA IgG with geometric mean titers (GMTs) of 3.5−4.6 × 10^3 on Day 14, and GMTs of 6.1−9.6 × 10^3 on Day 24 (Figure 3a). IgG titers were robustly boosted by the second dose of BNPs or LNPs, reaching GMTs of 5.6−7.5 × 10^5 on Day 43 and were maintained at high levels for the remainder of the study, albeit with a slight decline to a GMT of ∼3.3 × 10^5 on Day 154. Splenocytes were harvested at the final time point and restimulated with SIINFEKL peptide, which represents an immunodominant OVA $CD8^+$ T cell epitope.[37] IFNγ-producing $CD8^+$ T cells were detected only in vaccinated mice and were entirely $CD44^{hi}$ (see Figure 3b for representative FACS plots), indicating that they were OVA-specific, functional memory $CD8^+$ T cells. BNPs were more efficient than LNPs at inducing $CD8^+$ T cells, based on the significantly higher frequency of responders (average frequencies of 0.19 and 0.07% with respect to total viable leukocytes, respectively; Figure 3c). To evaluate the immunogenicity of the aged formulation, OVA mRNA-BNPs were stored in liquid format at 4 °C for 24 weeks (6 months) and then IM administered to mice based on the schedule above. Two doses of aged BNPs elicited OVA-specific $CD8^+$ T cells, identified using pentamer staining, that were entirely of the $CD44^{hi}$ activated/memory phenotype (see Figure 3d for representative FACS plots). Notably, the frequency of circulating $CD44^{hi}Pent^+CD8^+$ T cells generated by aged BNPs (0.5% with respect to total viable leukocytes) was significantly greater than the response induced by freshly fabricated LNPs (0.1%; Figure 3e). In terms of anti-OVA antibodies, both BNPs and LNPs elicited comparable levels of IgG at high titers (Figure 3f). Anti-PEG antibodies were implicated in the accelerated clearance and destabilization of PEGylated nanocarriers.[19] Based on the use of low molecular weight PEG (600 Da) in the fabrication of BNPs and the work by Steve Roffler and his team showing anti-PEG IgG and IgM to bind poorly to PEG molecules below 750 and 559 Da, respectively,[19] we hypothesized that BNPs may induce less anti-PEG antibodies compared to LNPs. Repeated IV doses of mRNA-LNPs boosted anti-PEG IgM and IgG to moderate levels on Day 28 (GMTs of 4178 and 1724, respectively; Figure 4a,b). In

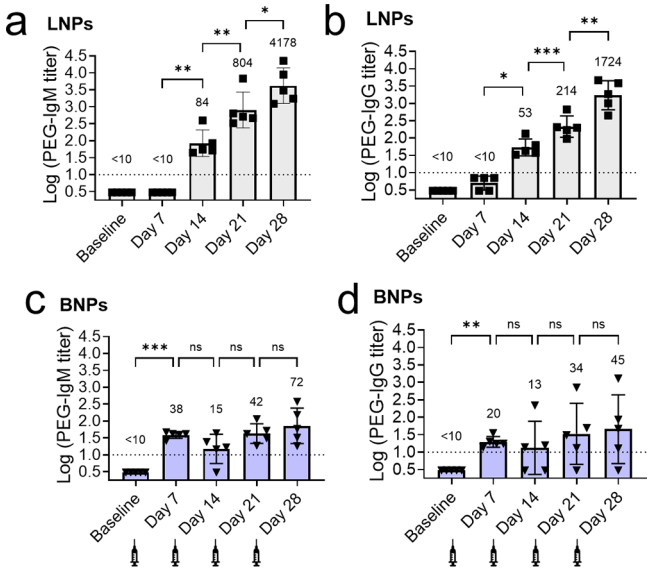

Figure 4. Repeated doses of mRNA-BNPs did not boost anti-PEG antibodies. (a−d) Mice (n = 5) were given four weekly IV injections (7 μg mRNA per dose), and serum PEG-specific antibodies were assessed 7 days after each injection. Geometric mean titers (GMTs) are indicated above the bar graphs. Horizontal dashed lines represent lower limits of detection (1:10 serum dilution). Syringes below the X-axis represent immunization time points. Repeated measures one-way ANOVA with Tukey's multiple comparisons is performed. *: $P \leq 0.05$; **: $P \leq 0.01$; ***: $P \leq 0.001$; ns, not significant.

contrast, a single dose of mRNA-BNPs elicited marginal anti-PEG IgM and IgG (GMTs of 38 and 20, respectively) that were not significantly boosted by subsequent injections (Figure 4c,d). In conclusion, we have shown mRNA-BNPs to efficiently induce an antigen-specific, but not carrier-specific, adaptive immune response. Moreover, its immunogenicity profile, relative to freshly fabricated LNPs, is preserved after prolonged storage at 4 °C. Together with the earlier observation that BNPs' physicochemical properties are maintained for 13 months at 4 °C, the incorporation of PBD-b-PEO in an LNP architecture clearly exerts a stabilizing effect while maintaining or enhancing different aspects of the antigen-specific immune response.

SARS-CoV-2 Spike mRNA-BNP Vaccine Protects Hamsters from Live Virus Challenge. The potential of BNPs for clinical application was assessed in a hamster model of nonlethal SARS-CoV-2 infection. BNPs encapsulating ancestral SARS-CoV-2 spike mRNA and an LNP comparator (Comirnaty biosimilar) were fabricated for this purpose. Golden Syrian hamsters were vaccinated SC or IM twice, 3 weeks apart, at a dose of 5 μg mRNA (Figure 5a). A single dose of mRNA-BNPs administered IM or SC generated comparable antispike IgG with a GMT of 2.4−2.9 × 10^3, which was slightly but not significantly different from the response elicited by the Comirnaty biosimilar (GMT of 5.0 × 10^3) administered IM (Figure 5b). Antibodies were strongly boosted by the second dose of mRNA-BNPs to a GMT of 1.6 × 10^4 after SC and 2.2 × 10^4 after IM and the response was not significantly different from that generated by the Comirnaty booster (GMT of 2.9 × 10^4). Hamsters were then challenged IN with a vaccine-matched virus to evaluate the protective efficacy of vaccination. Mock-vaccinated controls exhibited a progressive decline in body weight up to 9% of baseline values on Day 5 followed by recovery (Figure

https://doi.org/10.1021/acs.biomac.4c01820
Biomacromolecules XXXX, XXX, XXX−XXX

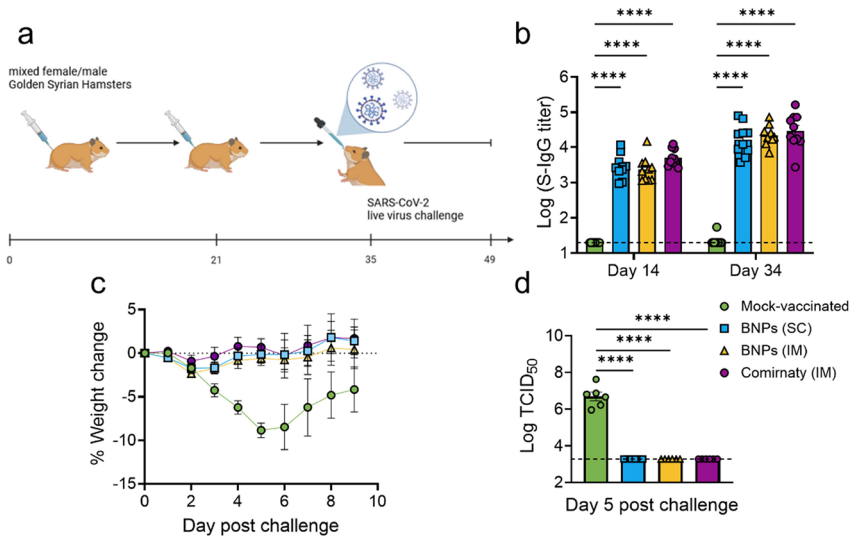

Figure 5. SARS-CoV-2 spike mRNA-BNPs are immunogenic and protective in hamsters. (a) Immunization and blood collection schedule. Golden Syrian hamsters (n = 10) were SC or IM injected with 5 μg of spike mRNA formulated in LNPs (i.e., Comirnaty biosimilar) or BNPs on Days 0 and 21. (b) Blood was collected on Days 21 (after first dose) and 34 (after second dose) for assessment of antispike serum IgG. (c) Changes in body weight with respect to baseline (Day 0) following the SARS-CoV-2 challenge. Mean ± SEM is shown. On Day 5, six animals were sacrificed after weight measurement to determine viral loads in their lungs. (d) Pulmonary viral loads. Infectious vial titers were expressed in terms of $TCID_{50}$. Horizontal dashed line represents the lower limit of detection. Samples below the limit are assigned a nominal value. Where appropriate, two-way repeated measures ANOVA or ordinary one-way ANOVA with Tukey's multiple comparisons is performed. Only significant differences are indicated. ****: $P \leq 0.0001$.

5c). BNP- and Comirnaty-vaccinated hamsters, in contrast, were well protected and exhibited stable body weights over the 9 day study (Figure 5c). Lungs harvested on Day 5 showed undetectable viral loads in hamsters vaccinated with BNPs or the Comirnaty biosimilar, whereas high viral titers at a geometric mean of 4.9×10^6 $TCID_{50}$ were detected in mock-vaccinated animals (Figure 5d). In conclusion, this study demonstrated equivalent in vivo protective efficacy between BNPs and the Comirnaty biosimilar.

DISCUSSION

Instability of LNPs can arise from lipid oxidation and/or hydrolysis, or the fusion/aggregation of particles during storage.[38] Accordingly, DLS measurements of mRNA-LNPs stored at 4 °C for 1 month reveal a broadening of its size distribution profile that suggests particle fusion or aggregation. Thermal stability can be improved through lyophilization, but successful application requires careful consideration of multiple parameters to avoid loss of efficacy after reconstitution. Another approach involves modifying the standard fabrication process to include a stabilizing component. A comparison of five structurally diverse ionizable lipids (C12−200, CKK-E12, MC3, SM-102, and lipid 23) incorporated into a standard LNP formulation, while preserving all other components, reveals C12−200 to be superior in maintaining the functionality of LNPs at 2−8 °C or room temperature for 11 weeks.[39] Similarly, a novel imidazole modified ionizable lipid combined with standard helper lipid DSPC, cholesterol, and DMG-PEG 2000 lipid generate stable nanoparticles that retain most of their in vivo bioactivity after 25 weeks of storage in PBS at 4 °C.[6] Amphiphilic block copolymers have played a vital role in the development of polymersomes, which exhibit reduced lateral mobility that translates to enhanced thermal stability, mechanical strength and rheological properties, as well as reduced drug permeability compared to liposomes.[22,40] Here, we have replaced DMG-PEG 2000 with PBD-*b*-PEO to markedly enhance the structural stability of the resultant nanoparticles for prolonged storage at 4 °C without affecting their function and immunogenicity. We have also shown that BNPs are deposited in secondary lymphoid organs and efficiently taken up by professional APCs. Among them, DCs are known to occupy a central role in the initiation of the adaptive immune response and the different subsets (pDCs, cDC1 and cDC2) efficiently take up BNPs, though the rate of uptake is greatest for cDC1. This subset is known for its ability to cross-present antigens required for $CD8^+$ T cell priming, hence driving an effective response against viruses and cancer.[41] Others have shown that protein antigens targeted to cDC1 by means of specific antibodies can generate potent humoral immune responses.[42,43] Accordingly, we have observed the induction of robust and durable antibody and $CD8^+$ T cell responses against OVA. Work is ongoing to evaluate mRNA-BNPs as a cancer therapy in a mouse model of melanoma.

BNPs exhibit lower mRNA loading concentration and lower organ transfection compared to LNPs yet our data clearly show mRNA-BNPs to remain highly immunogenic, as evidenced by the induction of an antigen-specific antibody response with a similar magnitude and longevity as LNPs, an antigen-specific $CD8^+$ T cell response that is significantly improved in terms of magnitude and longevity, and in vivo protective efficacy against SARS-CoV-2 that is comparable to that conferred by LNPs. While this may be driven, in part, by the preferential expression of mRNA-BNPs in secondary lymphoid organs and their efficient uptake by professional APCs, the reduced expression of mRNA-BNPs in the liver might also be key to understanding their increased immunogenicity. Notably, IM administered Luc mRNA-BNPs generate little to no expression in the liver whereas Luc mRNA-LNPs (Onpattro formulation) induce considerable liver expression that accounts for ∼40% of the total flux. Similar patterns of liver distribution have been

https://doi.org/10.1021/acs.biomac.4c01820
Biomacromolecules XXXX, XXX, XXX−XXX

reported for IM administered LNPs corresponding to Pfizer/BioNTech and Moderna formulations.[27] This is driven, in part, by the recruitment of apolipoprotein E (ApoE) to their biomolecular coronas that promote binding to low-density lipoprotein (LDL) receptors and other ApoE-binding receptors on hepatocytes.[25,27] The significance of liver distribution can be appreciated when one realizes its role in triggering immune tolerance. As an organ that constantly encounters dietary, commensal and exogenous antigens, the liver naturally mediates peripheral tolerance through multiple mechanisms, such as the interaction between LSECs and naïve $CD4^+$ T cells to generate regulatory T cells (Tregs).[44] Seen in this context, antigen expression in the liver may lead to an undesired dampening of the adaptive immune response. Restricting liver expression, such as through the use of BNPs, may improve vaccine potency by reducing liver-mediated tolerance to the antigen.[45]

The formation of a biomolecular corona on nanoparticles upon exposure to a biological fluid is a well-known phenomenon that governs the fate of nanoparticles, including their recognition by specific cell receptors and their interaction with specific cell types and organs.[46] As previously mentioned, the affinity of LNPs for the liver is driven partly by the adsorption of ApoE which promotes recognition by LDL receptors expressed by hepatocytes.[25] Based on the reduced uptake by hepatocytes and increased uptake by KCs seen in this work, we speculate that BNPs may generate a different biomolecular corona compared to LNPs. According to the landmark paper demonstrating critical thresholds for PEG content (2−5 wt %) and PEG length (2000−5000 Da) for polymeric nanoparticles to resist biomolecular corona formation,[47] BNPs with a PEG content of 1.64 wt % and PEG M_w of 600 Da would certainly generate a biomolecular corona when exposed to biological fluids. BNPs retain an appreciable level of liver targeting which implicates some degree of ApoE in their biomolecular corona, though their enhanced entry into a subset of KCs suggests the participation of yet-unknown constituents that may include complement proteins, immunoglobulins, albumin, fibrinogen, other glycoproteins and other apolipoproteins.[47−49] Based on the profile of high-low uptake of BNPs by KCs which contrasts with the intermediate, uniform uptake of LNPs, we speculate that phenotypically distinct subsets of KCs may exist that display different affinities for BNPs. In line with our hypothesis is a recent report of two phenotypically distinct KC subsets that are discriminated by the presence or absence of CD206, CD107b, LYVE-1, CD81, Bst2, CD63, and CD107a.[30] Here, we show that KCs with a high rate of BNP uptake express LYVE-1 at a markedly greater level than KCs with a low rate of uptake. Although our data do not establish the involvement of LYVE-1 in BNP uptake, it does suggest the involvement of entry receptors restricted to a subset of KCs. Putative candidates include CD206 (macrophage mannose receptor) and CD81 (host factor needed for hepatitis C virus and influenza virus infection).[30,50,51] Importantly, these receptors are not restricted to macrophages: CD206 is expressed by immature DCs and endothelial cells,[52] whereas CD81 is highly expressed by germinal center B cells.[53] Assuming the involvement of both receptors, they would also account for the uptake of BNPs by DCs and B cells and the increased level of targeting of secondary lymphoid organs seen in this work. In conclusion, we have identified putative receptors that may facilitate enhanced entry of BNPs into macrophages and possibly other APCs. Receptor recognition is likely mediated by the unique biomolecular corona that is expected to form spontaneously in vivo. As macrophages, DCs and B cells are key constituents of the secondary lymphoid organ, enhanced cellular uptake of BNPs would conceivably increase the expression of mRNA-BNPs in said organ. Profiling the biomolecular corona of BNPs and identifying their cellular entry receptors must be investigated further.

PEGylation is a widely used method to improve the stability and circulation kinetics of nanoparticles for drug and gene delivery, by shielding their surfaces from aggregation, opsonization, and phagocytosis.[54] Although weakly immunogenic, PEG can trigger an antibody response mediated largely by IgM and such antibodies are boosted by repeated administrations of PEG.[55,56] Anti-PEG antibodies have been associated with rapid clearance and destabilization of PEGylated nanoparticles, as well as the induction of hypersensitivity reactions.[55−59] Both BNPs and LNPs are immunogenic and evoke robust adaptive immune responses against the mRNA-encoded antigen, but only the former is inefficient at inducing anti-PEG antibodies. Unlike LNPs which are fabricated using methoxy-PEG (mPEG) of 2000 Da molecular weight, BNPs are composed of 600 Da hydroxyl-PEG (OH-PEG). The weak affinity of IgM and IgG for mPEG molecules lower than 559 and 750 Da, respectively, has been previously demonstrated.[19] Moreover, the terminal hydroxyl group is less immunogenic than the methoxy group, resulting in lower production of anti-PEG IgM antibodies.[60,61] Cumulatively, the use of low molecular weight OH-PEG in BNPs substantially lowers its ability to trigger anti-PEG antibodies, which is expected to improve its safety and efficacy following repeated administrations.

SARS-CoV-2 naïve individuals who have received two doses of Pfizer BNT162b2 or Moderna mRNA-1273 vaccine typically develop a durable cellular immune response that persists at least 6 months whereas antispike antibody levels rapidly decline.[62−64] In contrast, we observe mice vaccinated with OVA mRNA-LNPs to generate robust anti-OVA IgG that remains elevated more than 9 months postvaccination, whereas the levels of OVA-specific $CD8^+$ T cells have declined to baseline. The discrepancy between our mouse data and real-world human data remains unclear but may be due to antigen-specific effects and/or species-specific variation in the immune response. Nevertheless, in a head-to-head comparison of spike mRNA-BNPs and LNPs using a hamster model of SARS-CoV-2 infection, both formulations are fully protective against weight loss brought on by viral challenge and potently suppress pulmonary viral load. Based on the known efficacy of mRNA-LNP vaccines in the real world, we are therefore cautiously optimistic of the translatability of our preclinical findings.

CONCLUSIONS

The incorporation of amphiphilic block copolymer PBD-*b*-PEO into LNPs has markedly enhanced their morphological stability which enables prolonged storage in liquid format at 4 °C without negatively impacting their ability to deliver mRNA. As an mRNA vaccine, BNPs induce vigorous antigen-specific antibody and T cell responses and confer equivalent protection against SARS-CoV-2 as the Comirnaty biosimilar. These results demonstrate the potential clinical application of BNPs as a thermostable and immunogenic mRNA vaccine.

https://doi.org/10.1021/acs.biomac.4c01820
Biomacromolecules XXXX, XXX, XXX−XXX

■ ASSOCIATED CONTENT

Data Availability Statement

Data supporting the findings of this study is available from the corresponding author, Madhavan Nallani (mnallani@acmbiolabs.com), upon reasonable request.

Supporting Information

The Supporting Information is available free of charge at https://pubs.acs.org/doi/10.1021/acs.biomac.4c01820.

Size distributions of BNPs and LNPs before and after treatment with Triton X-100; differential uptake of BNPs by KCs (PDF)

■ AUTHOR INFORMATION

Corresponding Author

Madhavan Nallani − *ACM Biolabs Pte Ltd, Singapore 638075, Singapore; ACM Biosciences AG, 4051 Basel, Switzerland;* orcid.org/0009-0001-8583-3620; Phone: +65 6265 5646; Email: mnallani@acmbiolabs.com

Authors

Jian Hang Lam − *ACM Biolabs Pte Ltd, Singapore 638075, Singapore;* orcid.org/0000-0003-3378-350X

Gaurav Sinsinbar − *ACM Biolabs Pte Ltd, Singapore 638075, Singapore;* orcid.org/0000-0001-7720-7198

Ser Yue Loo − *ACM Biolabs Pte Ltd, Singapore 638075, Singapore*

Teck Wan Chia − *ACM Biolabs Pte Ltd, Singapore 638075, Singapore*

Yan Jun Lee − *ACM Biolabs Pte Ltd, Singapore 638075, Singapore*

Jing Yi Fong − *ACM Biolabs Pte Ltd, Singapore 638075, Singapore*

Yoong Eng Chia − *ACM Biolabs Pte Ltd, Singapore 638075, Singapore*

Rocco Roberto Penna − *Department of Dermatology, University Hospital Zurich (USZ), University of Zurich (UZH), 8091 Zurich, Switzerland; Faculty of Science, University of Zurich, 8006 Zurich, Switzerland;* orcid.org/0009-0007-9784-016X

Shaoqiong Liu − *ACM Biolabs Pte Ltd, Singapore 638075, Singapore*

Steve Pascolo − *Department of Dermatology, University Hospital Zurich (USZ), University of Zurich (UZH), 8091 Zurich, Switzerland; Faculty of Science, University of Zurich, 8006 Zurich, Switzerland*

Katherine Schultheis − *ACM Biosciences AG, 4051 Basel, Switzerland;* orcid.org/0000-0001-9232-1888

Complete contact information is available at: https://pubs.acs.org/10.1021/acs.biomac.4c01820

Author Contributions

The manuscript was written through contributions of all authors. All authors have given approval to the final version of the manuscript.

Funding

This project was supported in part by Innosuisse ("Development of a novel delivery system for mRNA COVID-19 vaccines", application no. 52910.1 IP-LS).

Notes

The authors declare the following competing financial interest(s): J.H.L., G.S., S.Y.L., T.W.C., Y.J.L., J.Y.F., Y.E.C., S.Q.L., K.S. and M.N. were employed under ACM Biolabs Pte Ltd at the time of writing. The ATP formulation described in this work was patented under International Application No. PCT/EP2023/054613.

■ ACKNOWLEDGMENTS

We would like to thank Dr. Graham Taylor (President at Helix Biotech, Inc.) for the fabrication of the Comirnaty biosimilar, and Dr. Huaqiong Li (Wenzhou Institute, University of Chinese Academy of Sciences, China) and his team for bioluminescence imaging studies.

■ ABBREVIATIONS

BNP, block copolymer nanoparticle; PBD-*b*-PEO, polybutadiene-*b*-poly(ethylene glycol); OVA, ovalbumin; IgG, immunoglobulin G; IgM, immunoglobulin M; PEG, polyethylene glycol; LNPs, lipid nanoparticles; mRNA, messenger ribonucleic acid; COVID-19, coronavirus disease 2019; SARS-CoV-2, severe acute respiratory syndrome coronavirus 2

■ REFERENCES

(1) Fiolet, T.; Kherabi, Y.; MacDonald, C. J.; Ghosn, J.; Peiffer-Smadja, N. Comparing COVID-19 vaccines for their characteristics, efficacy and effectiveness against SARS-CoV-2 and variants of concern: a narrative review. *Clin Microbiol Infect* **2022**, *28* (2), 202−221.

(2) El Sahly, H. M.; Baden, L. R.; Essink, B.; Doblecki-Lewis, S.; Martin, J. M.; Anderson, E. J.; Campbell, T. B.; Clark, J.; Jackson, L. A.; Fichtenbaum, C. J.; Zervos, M.; Rankin, B.; Eder, F.; Feldman, G.; Kennelly, C.; Han-Conrad, L.; Levin, M.; Neuzil, K. M.; Corey, L.; Gilbert, P.; Janes, H.; Follmann, D.; Marovich, M.; Polakowski, L.; Mascola, J. R.; Ledgerwood, J. E.; Graham, B. S.; August, A.; Clouting, H.; Deng, W.; Han, S.; Leav, B.; Manzo, D.; Pajon, R.; Schödel, F.; Tomassini, J. E.; Zhou, H.; Miller, J. Efficacy of the mRNA-1273 SARS-CoV-2 Vaccine at Completion of Blinded Phase. *N Engl J. Med.* **2021**, *385* (19), 1774−1785.

(3) Frenck, R. W., Jr.; Klein, N. P.; Kitchin, N.; Gurtman, A.; Absalon, J.; Lockhart, S.; Perez, J. L.; Walter, E. B.; Senders, S.; Bailey, R.; Swanson, K. A.; Ma, H.; Xu, X.; Koury, K.; Kalina, W. V.; Cooper, D.; Jennings, T.; Brandon, D. M.; Thomas, S. J.; Türeci, Ö.; Tresnan, D. B.; Mather, S.; Dormitzer, P. R.; Şahin, U.; Jansen, K. U.; Gruber, W. C. Safety, Immunogenicity, and Efficacy of the BNT162b2 Covid-19 Vaccine in Adolescents. *N Engl J. Med.* **2021**, *385* (3), 239−250.

(4) Thomas, S. J.; Moreira, E. D., Jr.; Kitchin, N.; Absalon, J.; Gurtman, A.; Lockhart, S.; Perez, J. L.; Pérez Marc, G.; Polack, F. P.; Zerbini, C.; Bailey, R.; Swanson, K. A.; Xu, X.; Roychoudhury, S.; Koury, K.; Bouguermouh, S.; Kalina, W. V.; Cooper, D.; Frenck, R. W., Jr; Hammitt, L. L.; Türeci, Ö.; Nell, H.; Schaefer, A.; Ünal, S.; Yang, Q.; Liberator, P.; Tresnan, D. B.; Mather, S.; Dormitzer, P. R.; Şahin, U.; Gruber, W. C.; Jansen, K. U. Safety and Efficacy of the BNT162b2 mRNA Covid-19 Vaccine through 6 Months. *N Engl J. Med.* **2021**, *385* (19), 1761−1773.

(5) Baden, L. R.; El Sahly, H. M.; Essink, B.; Kotloff, K.; Frey, S.; Novak, R.; Diemert, D.; Spector, S. A.; Rouphael, N.; Creech, C. B.; McGettigan, J.; Khetan, S.; Segall, N.; Solis, J.; Brosz, A.; Fierro, C.; Schwartz, H.; Neuzil, K.; Corey, L.; Gilbert, P.; Janes, H.; Follmann, D.; Marovich, M.; Mascola, J.; Polakowski, L.; Ledgerwood, J.; Graham, B. S.; Bennett, H.; Pajon, R.; Knightly, C.; Leav, B.; Deng, W.; Zhou, H.; Han, S.; Ivarsson, M.; Miller, J.; Zaks, T. Efficacy and Safety of the mRNA-1273 SARS-CoV-2 Vaccine. *N. Engl. J. Med.* **2021**, *384* (5), 403−416.

(6) Ripoll, M.; Bernard, M. C.; Vaure, C.; Bazin, E.; Commandeur, S.; Perkov, V.; Lemdani, K.; Nicolaï, M. C.; Bonifassi, P.; Kichler, A.; Frisch, B.; Haensler, J. An imidazole modified lipid confers enhanced mRNA-LNP stability and strong immunization properties in mice and non-human primates. *Biomaterials* **2022**, *286*, No. 121570.

(7) Gerhardt, A.; Voigt, E.; Archer, M.; Reed, S.; Larson, E.; Van Hoeven, N.; Kramer, R.; Fox, C.; Casper, C. A flexible, thermostable nanostructured lipid carrier platform for RNA vaccine delivery. *Mol. Ther Methods Clin Dev* **2022**, *25*, 205−214.
(8) Voigt, E. A.; Gerhardt, A.; Hanson, D.; Jennewein, M. F.; Battisti, P.; Reed, S.; Singh, J.; Mohamath, R.; Bakken, J.; Beaver, S.; Press, C.; Soon-Shiong, P.; Paddon, C. J.; Fox, C. B.; Casper, C. A self-amplifying RNA vaccine against COVID-19 with long-term room-temperature stability. *NPJ. Vaccines* **2022**, *7* (1), 136.
(9) Kim, B.; Hosn, R. R.; Remba, T.; Yun, D.; Li, N.; Abraham, W.; Melo, M. B.; Cortes, M.; Li, B.; Zhang, Y.; Dong, Y.; Irvine, D. J. Optimization of storage conditions for lipid nanoparticle-formulated self-replicating RNA vaccines. *J. Controlled Release* **2023**, *353*, 241−253.
(10) Ball, R. L.; Bajaj, P.; Whitehead, K. A. Achieving long-term stability of lipid nanoparticles: examining the effect of pH, temperature, and lyophilization. *Int. J. Nanomedicine* **2017**, *12*, 305−315.
(11) Uddin, M. N.; Roni, M. A. Challenges of Storage and Stability of mRNA-Based COVID-19 Vaccines. *Vaccines (Basel)* **2021**, *9* (9), 1033.
(12) Ai, L.; Li, Y.; Zhou, L.; Yao, W.; Zhang, H.; Hu, Z.; Han, J.; Wang, W.; Wu, J.; Xu, P.; Wang, R.; Li, Z.; Li, Z.; Wei, C.; Liang, J.; Chen, H.; Yang, Z.; Guo, M.; Huang, Z.; Wang, X.; Zhang, Z.; Xiang, W.; Sun, D.; Xu, L.; Huang, M.; Lv, B.; Peng, P.; Zhang, S.; Ji, X.; Luo, H.; Chen, N.; Chen, J.; Lan, K.; Hu, Y. Lyophilized mRNA-lipid nanoparticle vaccines with long-term stability and high antigenicity against SARS-CoV-2. *Cell Discov* **2023**, *9* (1), 9.
(13) Muramatsu, H.; Lam, K.; Bajusz, C.; Laczkó, D.; Karikó, K.; Schreiner, P.; Martin, A.; Lutwyche, P.; Heyes, J.; Pardi, N. Lyophilization provides long-term stability for a lipid nanoparticle-formulated, nucleoside-modified mRNA vaccine. *Mol. Ther* **2022**, *30* (5), 1941−1951.
(14) Go, Y. K.; Leal, C. Polymer-Lipid Hybrid Materials. *Chem. Rev.* **2021**, *121* (22), 13996−14030.
(15) Sivadasan, D.; Sultan, M. H.; Madkhali, O.; Almoshari, Y.; Thangavel, N. Polymeric Lipid Hybrid Nanoparticles (PLNs) as Emerging Drug Delivery Platform-A Comprehensive Review of Their Properties Preparation Methods, and Therapeutic Applications. *Pharmaceutics* **2021**, *13* (8), 1291.
(16) Ottonelli, I.; Baraldi, C.; Ruozi, B.; Vandelli, M. A.; Tosi, G.; Duskey, J. T. Advantages and challenges of polymer-lipid hybrid nanoparticles for the delivery of biotech drugs. *Nanomedicine (Lond)* **2025**, 1−3.
(17) Lam, J. H.; Khan, A. K.; Cornell, T. A.; Chia, T. W.; Dress, R. J.; Yeow, W. W. W.; Mohd-Ismail, N. K.; Venkataraman, S.; Ng, K. T.; Tan, Y. J.; Anderson, D. E.; Ginhoux, F.; Nallani, M. Polymersomes as Stable Nanocarriers for a Highly Immunogenic and Durable SARS-CoV-2 Spike Protein Subunit Vaccine. *ACS Nano* **2021**, *15* (10), 15754−15770.
(18) Lam, J. H.; Shivhare, D.; Chia, T. W.; Chew, S. L.; Sinsinbar, G.; Aw, T. Y.; Wong, S.; Venkataraman, S.; Lim, F. W. I.; Vandepapeliere, P.; Nallani, M. Artificial Cell Membrane Polymersome-Based Intranasal Beta Spike Formulation as a Second Generation Covid-19 Vaccine. *ACS Nano* **2022**, *16* (10), 16757−16775.
(19) Chen, B. M.; Cheng, T. L.; Roffler, S. R. Polyethylene Glycol Immunogenicity: Theoretical, Clinical, and Practical Aspects of Anti-Polyethylene Glycol Antibodies. *ACS Nano* **2021**, *15* (9), 14022−14048.
(20) Yardeni, T.; Eckhaus, M.; Morris, H. D.; Huizing, M.; Hoogstraten-Miller, S. Retro-orbital injections in mice. *Lab Anim (NY)* **2011**, *40* (5), 155−160.
(21) Yang, Q.; Jacobs, T. M.; McCallen, J. D.; Moore, D. T.; Huckaby, J. T.; Edelstein, J. N.; Lai, S. K. Analysis of Pre-existing IgG and IgM Antibodies against Polyethylene Glycol (PEG) in the General Population. *Anal. Chem.* **2016**, *88* (23), 11804−11812.
(22) Sinsinbar, G.; Bindra, A. K.; Liu, S.; Chia, T. W.; Yoong Eng, E. C.; Loo, S. Y.; Lam, J. H.; Schultheis, K.; Nallani, M. Amphiphilic Block Copolymer Nanostructures as a Tunable Delivery Platform: Perspective and Framework for the Future Drug Product Development. *Biomacromolecules* **2024**, *25* (2), 541−563.
(23) Gettel, D. L.; Sanborn, J.; Patel, M. A.; de Hoog, H. P.; Liedberg, B.; Nallani, M.; Parikh, A. N. Mixing, diffusion, and percolation in binary supported membranes containing mixtures of lipids and amphiphilic block copolymers. *J. Am. Chem. Soc.* **2014**, *136* (29), 10186−10189.
(24) Le Meins, J. F.; Schatz, C.; Lecommandoux, S.; Sandre, O. Hybrid polymer/lipid vesicles: state of the art and future perspectives. *Mater. Today* **2013**, *16* (10), 397−402.
(25) Akinc, A.; Querbes, W.; De, S.; Qin, J.; Frank-Kamenetsky, M.; Jayaprakash, K. N.; Jayaraman, M.; Rajeev, K. G.; Cantley, W. L.; Dorkin, J. R.; Butler, J. S.; Qin, L.; Racie, T.; Sprague, A.; Fava, E.; Zeigerer, A.; Hope, M. J.; Zerial, M.; Sah, D. W. Y.; Fitzgerald, K.; Tracy, M. A.; Manoharan, M.; Koteliansky, V.; de Fougerolles, A.; Maier, M. A. Targeted delivery of RNAi therapeutics with endogenous and exogenous ligand-based mechanisms. *Mol. Ther.* **2010**, *18* (7), 1357−1364.
(26) Su, K.; Shi, L.; Sheng, T.; Yan, X.; Lin, L.; Meng, C.; Wu, S.; Chen, Y.; Zhang, Y.; Wang, C.; Wang, Z.; Qiu, J.; Zhao, J.; Xu, T.; Ping, Y.; Gu, Z.; Liu, S. Reformulating lipid nanoparticles for organ-targeted mRNA accumulation and translation. *Nat. Commun.* **2024**, *15* (1), 5659.
(27) Pateev, I.; Seregina, K.; Ivanov, R.; Reshetnikov, V. Biodistribution of RNA Vaccines and of Their Products: Evidence from Human and Animal Studies. *Biomedicines* **2024**, *12* (1), 59.
(28) Liu, Z.; Gu, Y.; Shin, A.; Zhang, S.; Ginhoux, F. Analysis of Myeloid Cells in Mouse Tissues with Flow Cytometry. *STAR Protoc* **2020**, *1* (1), No. 100029.
(29) Blériot, C.; Ginhoux, F. Understanding the Heterogeneity of Resident Liver Macrophages. *Front Immunol* **2019**, *10*, 2694.
(30) Blériot, C.; Barreby, E.; Dunsmore, G.; Ballaire, R.; Chakarov, S.; Ficht, X.; De Simone, G.; Andreata, F.; Fumagalli, V.; Guo, W.; Wan, G.; Gessain, G.; Khalilnezhad, A.; Zhang, X. M.; Ang, N.; Chen, P.; Morgantini, C.; Azzimato, V.; Kong, W. T.; Liu, Z.; Pai, R.; Lum, J.; Foo, S.; Low, I.; Xu, C.; Malleret, B.; Kairi, M. F. M.; Balachander, A.; Cexus, O.; Larbi, A.; Lee, B.; Newell, E. W.; Ng, L. G.; Phoo, W. W.; Sobota, R. M.; Sharma, A.; Howland, S. W.; Chen, J.; Bajenoff, M.; Yvan-Charvet, L.; Venteclef, N.; Iannacone, M.; Aouadi, M.; Ginhoux, F. A subset of Kupffer cells regulates metabolism through the expression of CD36. *Immunity* **2021**, *54* (9), 2101−2116.e6.
(31) Vogel, A. B.; Kanevsky, I.; Che, Y.; Swanson, K. A.; Muik, A.; Vormehr, M.; Kranz, L. M.; Walzer, K. C.; Hein, S.; Güler, A.; Loschko, J.; Maddur, M. S.; Ota-Setlik, A.; Tompkins, K.; Cole, J.; Lui, B. G.; Ziegenhals, T.; Plaschke, A.; Eisel, D.; Dany, S. C.; Fesser, S.; Erbar, S.; Bates, F.; Schneider, D.; Jesionek, B.; Sänger, B.; Wallisch, A.; Feuchter, Y.; Junginger, H.; Krumm, S. A.; Heinen, A. P.; Adams-Quack, P.; Schlereth, J.; Schille, S.; Kröner, C.; De La Caridad Güimil Garcia, R.; Hiller, T.; Fischer, L.; Sellers, R. S.; Choudhary, S.; Gonzalez, O.; Vascotto, F.; Gutman, M. R.; Fontenot, J. A.; Hall-Ursone, S.; Brasky, K.; Griffor, M. C.; Han, S.; Su, A. A. H.; Lees, J. A.; Nedoma, N. L.; Mashalidis, E. H.; Sahasrabudhe, P. V.; Tan, C. Y.; Pavliakova, D.; Singh, G.; Fontes-Garfias, C.; Pride, M.; Scully, I. L.; Ciolino, T.; Obregon, J.; Gazi, M.; Carrion, R., Jr; Alfson, K. J.; Kalina, W. V.; Kaushal, D.; Shi, P. Y.; Klamp, T.; Rosenbaum, C.; Kuhn, A. N.; Türeci, Ö.; Dormitzer, P. R.; Jansen, K. U.; Sahin, U. BNT162b vaccines protect rhesus macaques from SARS-CoV-2. *Nature* **2021**, *592* (7853), 283−289.
(32) Wu, K.; Choi, A.; Koch, M.; Elbashir, S.; Ma, L.; Lee, D.; Woods, A.; Henry, C.; Palandjian, C.; Hill, A.; Jani, H.; Quinones, J.; Nunna, N.; O'Connell, S.; McDermott, A. B.; Falcone, S.; Narayanan, E.; Colpitts, T.; Bennett, H.; Corbett, K. S.; Seder, R.; Graham, B. S.; Stewart-Jones, G. B. E.; Carfi, A.; Edwards, D. K. Variant SARS-CoV-2 mRNA vaccines confer broad neutralization as primary or booster series in mice. *Vaccine* **2021**, *39* (51), 7394−7400.
(33) Pardi, N.; Tuyishime, S.; Muramatsu, H.; Kariko, K.; Mui, B. L.; Tam, Y. K.; Madden, T. D.; Hope, M. J.; Weissman, D. Expression

https://doi.org/10.1021/acs.biomac.4c01820
Biomacromolecules XXXX, XXX, XXX−XXX

kinetics of nucleoside-modified mRNA delivered in lipid nanoparticles to mice by various routes. *J. Controlled Release* **2015**, *217*, 345−351.
(34) DiPiazza, A. T.; Leist, S. R.; Abiona, O. M.; Moliva, J. I.; Werner, A.; Minai, M.; Nagata, B. M.; Bock, K. W.; Phung, E.; Schäfer, A.; Dinnon, K. H., 3rd; Chang, L. A.; Loomis, R. J.; Boyoglu-Barnum, S.; Alvarado, G. S.; Sullivan, N. J.; Edwards, D. K.; Morabito, K. M.; Mascola, J. R.; Carfi, A.; Corbett, K. S.; Moore, I. N.; Baric, R. S.; Graham, B. S.; Ruckwardt, T. J. COVID-19 vaccine mRNA-1273 elicits a protective immune profile in mice that is not associated with vaccine-enhanced disease upon SARS-CoV-2 challenge. *Immunity* **2021**, *54* (8), 1869−1882.e6.
(35) Meyer, M.; Wang, Y.; Edwards, D.; Smith, G. R.; Rubenstein, A. B.; Ramanathan, P.; Mire, C. E.; Pietzsch, C.; Chen, X.; Ge, Y.; Cheng, W. S.; Henry, C.; Woods, A.; Ma, L.; Stewart-Jones, G. B.; Bock, K. W.; Minai, M.; Nagata, B. M.; Periasamy, S.; Shi, P. Y.; Graham, B. S.; Moore, I. N.; Ramos, I.; Troyanskaya, O. G.; Zaslavsky, E.; Carfi, A.; Sealfon, S. C.; Bukreyev, A. Attenuated activation of pulmonary immune cells in mRNA-1273-vaccinated hamsters after SARS-CoV-2 infection. *J. Clin. Invest.* **2021**, *131* (20), No. e148036.
(36) Schoenmaker, L.; Witzigmann, D.; Kulkarni, J. A.; Verbeke, R.; Kersten, G.; Jiskoot, W.; Crommelin, D. J. A. mRNA-lipid nanoparticle COVID-19 vaccines: Structure and stability. *Int. J. Pharm.* **2021**, *601*, No. 120586.
(37) Karandikar, S. H.; Sidney, J.; Sette, A.; Selby, M. J.; Korman, A. J.; Srivastava, P. K. New epitopes in ovalbumin provide insights for cancer neoepitopes. *JCI Insight* **2019**, *5* (8), No. e127882.
(38) Fan, Y.; Marioli, M.; Zhang, K. Analytical characterization of liposomes and other lipid nanoparticles for drug delivery. *J. Pharm. Biomed Anal* **2021**, *192*, No. 113642.
(39) Reinhart, A. G.; Osterwald, A.; Ringler, P.; Leiser, Y.; Lauer, M. E.; Martin, R. E.; Ullmer, C.; Schumacher, F.; Korn, C.; Keller, M. Investigations into mRNA Lipid Nanoparticles Shelf-Life Stability under Nonfrozen Conditions. *Mol. Pharmaceutics* **2023**, *20* (12), 6492−6503.
(40) Rideau, E.; Dimova, R.; Schwille, P.; Wurm, F. R.; Landfester, K. Liposomes and polymersomes: a comparative review towards cell mimicking. *Chem. Soc. Rev.* **2018**, *47* (23), 8572−8610.
(41) Theisen, D.; Murphy, K. The role of cDC1s in vivo: CD8 T cell priming through cross-presentation. *F1000Res.* **2017**, *6* (98), 98.
(42) Fossum, E.; Tesfaye, D. Y.; Bobic, S.; Gudjonsson, A.; Braathen, R.; Lahoud, M. H.; Caminschi, I.; Bogen, B. Targeting Antigens to Different Receptors on Conventional Type 1 Dendritic Cells Impacts the Immune Response. *J. Immunol* **2020**, *205* (3), 661−673.
(43) Lahoud, M. H.; Ahmet, F.; Kitsoulis, S.; Wan, S. S.; Vremec, D.; Lee, C. N.; Phipson, B.; Shi, W.; Smyth, G. K.; Lew, A. M.; Kato, Y.; Mueller, S. N.; Davey, G. M.; Heath, W. R.; Shortman, K.; Caminschi, I. Targeting antigen to mouse dendritic cells via Clec9A induces potent CD4 T cell responses biased toward a follicular helper phenotype. *J. Immunol* **2011**, *187* (2), 842−850.
(44) Kusumoputro, S.; Au, C.; Lam, K. H.; Park, N.; Hyun, A.; Kusumoputro, E.; Wang, X.; Xia, T. Liver-Targeting Nanoplatforms for the Induction of Immune Tolerance. *Nanomaterials (Basel)* **2024**, *14* (1), 67.
(45) Parrett, B. J.; Yamaoka, S.; Barry, M. A. Reducing off-target expression of mRNA therapeutics and vaccines in the liver with microRNA binding sites. *Mol. Ther Methods Clin Dev* **2025**, *33* (1), No. 101402.
(46) Aliyandi, A.; Zuhorn, I. S.; Salvati, A. Disentangling Biomolecular Corona Interactions With Cell Receptors and Implications for Targeting of Nanomedicines. *Front Bioeng Biotechnol* **2020**, *8*, No. 599454.
(47) Gref, R.; Lück, M.; Quellec, P.; Marchand, M.; Dellacherie, E.; Harnisch, S.; Blunk, T.; Müller, R. H. 'Stealth' corona-core nanoparticles surface modified by polyethylene glycol (PEG): influences of the corona (PEG chain length and surface density) and of the core composition on phagocytic uptake and plasma protein adsorption. *Colloids Surf. B Biointerfaces* **2000**, *18* (3−4), 301−313.
(48) Trinh, D. N.; Gardner, R. A.; Franciosi, A. N.; McCarthy, C.; Keane, M. P.; Soliman, M. G.; O'Donnell, J. S.; Meleady, P.; Spencer, D. I. R.; Monopoli, M. P. Nanoparticle Biomolecular Corona-Based Enrichment of Plasma Glycoproteins for N-Glycan Profiling and Application in Biomarker Discovery. *ACS Nano* **2022**, *16* (4), 5463−5475.
(49) Bertrand, N.; Grenier, P.; Mahmoudi, M.; Lima, E. M.; Appel, E. A.; Dormont, F.; Lim, J. M.; Karnik, R.; Langer, R.; Farokhzad, O. C. Mechanistic understanding of in vivo protein corona formation on polymeric nanoparticles and impact on pharmacokinetics. *Nat. Commun.* **2017**, *8* (1), 777.
(50) Zhang, J.; Randall, G.; Higginbottom, A.; Monk, P.; Rice, C. M.; McKeating, J. A. CD81 is required for hepatitis C virus glycoprotein-mediated viral infection. *J. Virol* **2004**, *78* (3), 1448−1455.
(51) He, J.; Sun, E.; Bujny, M. V.; Kim, D.; Davidson, M. W.; Zhuang, X. Dual function of CD81 in influenza virus uncoating and budding. *PLoS Pathog* **2013**, *9* (10), No. e1003701.
(52) Tanaka, S.; Ohgidani, M.; Hata, N.; Inamine, S.; Sagata, N.; Shirouzu, N.; Mukae, N.; Suzuki, S. O.; Hamasaki, H.; Hatae, R.; Sangatsuda, Y.; Fujioka, Y.; Takigawa, K.; Funakoshi, Y.; Iwaki, T.; Hosoi, M.; Iihara, K.; Mizoguchi, M.; Kato, T. A. CD206 Expression in Induced Microglia-Like Cells From Peripheral Blood as a Surrogate Biomarker for the Specific Immune Microenvironment of Neurosurgical Diseases Including Glioma. *Front Immunol* **2021**, *12*, No. 670131.
(53) Luo, R. F.; Zhao, S.; Tibshirani, R.; Myklebust, J. H.; Sanyal, M.; Fernandez, R.; Gratzinger, D.; Marinelli, R. J.; Lu, Z. S.; Wong, A.; Levy, R.; Levy, S.; Natkunam, Y. CD81 protein is expressed at high levels in normal germinal center B cells and in subtypes of human lymphomas. *Hum Pathol* **2010**, *41* (2), 271−280.
(54) Suk, J. S.; Xu, Q.; Kim, N.; Hanes, J.; Ensign, L. M. PEGylation as a strategy for improving nanoparticle-based drug and gene delivery. *Adv. Drug Deliv. Rev.* **2016**, *99* (Pt A), 28−51.
(55) Besin, G.; Milton, J.; Sabnis, S.; Howell, R.; Mihai, C.; Burke, K.; Benenato, K. E.; Stanton, M.; Smith, P.; Senn, J.; Hoge, S. Accelerated Blood Clearance of Lipid Nanoparticles Entails a Biphasic Humoral Response of B-1 Followed by B-2 Lymphocytes to Distinct Antigenic Moieties. *Immunohorizons* **2019**, *3* (7), 282−293.
(56) Wang, H.; Wang, Y.; Yuan, C.; Xu, X.; Zhou, W.; Huang, Y.; Lu, H.; Zheng, Y.; Luo, G.; Shang, J.; Sui, M. Polyethylene glycol (PEG)-associated immune responses triggered by clinically relevant lipid nanoparticles in rats. *NPJ. Vaccines* **2023**, *8* (1), 169.
(57) Estapé Senti, M.; de Jongh, C. A.; Dijkxhoorn, K.; Verhoef, J. J. F.; Szebeni, J.; Storm, G.; Hack, C. E.; Schiffelers, R. M.; Fens, M. H.; Boross, P. Anti-PEG antibodies compromise the integrity of PEGylated lipid-based nanoparticles via complement. *J. Controlled Release* **2022**, *341*, 475−486.
(58) Judge, A.; McClintock, K.; Phelps, J. R.; Maclachlan, I. Hypersensitivity and loss of disease site targeting caused by antibody responses to PEGylated liposomes. *Mol. Ther* **2006**, *13* (2), 328−337.
(59) Zhao, Y.; Wang, L.; Yan, M.; Ma, Y.; Zang, G.; She, Z.; Deng, Y. Repeated injection of PEGylated solid lipid nanoparticles induces accelerated blood clearance in mice and beagles. *Int. J. Nanomedicine* **2012**, *7*, 2891−2900.
(60) Sherman, M. R.; Williams, L. D.; Sobczyk, M. A.; Michaels, S. J.; Saifer, M. G. Role of the methoxy group in immune responses to mPEG-protein conjugates. *Bioconjug Chem.* **2012**, *23* (3), 485−499.
(61) Saifer, M. G.; Williams, L. D.; Sobczyk, M. A.; Michaels, S. J.; Sherman, M. R. Selectivity of binding of PEGs and PEG-like oligomers to anti-PEG antibodies induced by methoxyPEG-proteins. *Mol. Immunol* **2014**, *57* (2), 236−246.
(62) Pitiriga, V. C.; Papamentzelopoulou, M.; Konstantinakou, K. E.; Vasileiou, I. V.; Konstantinidis, A. D.; Spyrou, N. I.; Tsakris, A. Prolonged SARS-CoV-2 T Cell Responses in a Vaccinated COVID-19-Naive Population. *Vaccines (Basel)* **2024**, *12* (3), 270.
(63) Goel, R. R.; Painter, M. M.; Apostolidis, S. A.; Mathew, D.; Meng, W.; Rosenfeld, A. M.; Lundgreen, K. A.; Reynaldi, A.; Khoury, D. S.; Pattekar, A.; Gouma, S.; Kuri-Cervantes, L.; Hicks, P.; Dysinger,

https://doi.org/10.1021/acs.biomac.4c01820
Biomacromolecules XXXX, XXX, XXX−XXX

S.; Hicks, A.; Sharma, H.; Herring, S.; Korte, S.; Baxter, A. E.; Oldridge, D. A.; Giles, J. R.; Weirick, M. E.; McAllister, C. M.; Awofolaju, M.; Tanenbaum, N.; Drapeau, E. M.; Dougherty, J.; Long, S.; D'Andrea, K.; Hamilton, J. T.; McLaughlin, M.; Williams, J. C.; Adamski, S.; Kuthuru, O.; Frank, I.; Betts, M. R.; Vella, L. A.; Grifoni, A.; Weiskopf, D.; Sette, A.; Hensley, S. E.; Davenport, M. P.; Bates, P.; Luning Prak, E. T.; Greenplate, A. R.; Wherry, E. J. mRNA vaccines induce durable immune memory to SARS-CoV-2 and variants of concern. *Science* **2021**, *374* (6572), No. abm0829.

(64) Guerrera, G.; Picozza, M.; D'Orso, S.; Placido, R.; Pirronello, M.; Verdiani, A.; Termine, A.; Fabrizio, C.; Giannessi, F.; Sambucci, M.; Balice, M. P.; Caltagirone, C.; Salvia, A.; Rossini, A.; Battistini, L.; Borsellino, G. BNT162b2 vaccination induces durable SARS-CoV-2-specific T cells with a stem cell memory phenotype. *Sci. Immunol* **2021**, *6* (66), No. eabl5344.

https://doi.org/10.1021/acs.biomac.4c01820
Biomacromolecules XXXX, XXX, XXX−XXX